

SCATTEROMETER IMAGE RECONSTRUCTION FROM APERTURE-FILTERED SAMPLES

Brent A. Williams and David G. Long

Brigham Young University, MERS Laboratory 459 CB, Provo, UT 84602

ABSTRACT

This paper considers sampling and reconstruction theory with application to scatterometer image reconstruction. Backscatter imaging is approached as the inversion of a noisy aperture-filtered sampling operation. A reconstruction estimator based on maximum a posteriori probability (MAP) estimation is proposed to recover the conventional samples from noisy aperture-filtered samples. Examples from the SeaWinds scatterometer and the Advanced Wind Scatterometer (ASCAT) are presented.

1. INTRODUCTION

A scatterometer is an active microwave radar that measures the normalized radar cross section (σ^0) averaged spatially over an aperture function. Typically, each radar pulse is partitioned into several measurements using range-Doppler processing so the spatial aperture function of each measurement is a combination of the antenna footprint and range-Doppler processing. The sampling geometry results in irregularly spaced aperture functions with different shapes. A scatterometer makes several measurements with different azimuth angles, incidence angles, and possibly polarizations of the same spatial region.

Since scatterometers make multiple overlapping measurements of the Earth's surface, these measurements may be combined to produce σ^0 images. Several imaging methods have been proposed for scatterometer image reconstruction. Perhaps the most simple is to create a gridded product by averaging all measurements whose centers fall into a particular grid element. Gridding produces relatively low resolution images. Another imaging technique employs a weighted average on a higher resolution grid. This is the basis of the averaging (AVE) algorithm [1], which sets each pixel to the average of all the σ^0 measurements, weighted by the value of the respective aperture functions at each pixel. Some common methods that further enhance the resolution are based on the additive algebraic reconstruction technique (AART) or the multiplicative algebraic reconstruction technique (MART) [1] [2]. For the noisy scatterometer σ^0 imaging problem, the MART algorithm tends to produce a less noisy estimate of the conventional samples than the AART algorithm. This

led to the scatterometer image reconstruction (SIR) algorithm, which is a normalized version of MART that tends to converge faster with less noise [1] [2].

Scatterometer σ^0 imaging algorithms proposed in the literature [1] [2] are based on noise-free reconstruction operators and do not use knowledge of the noise distribution. Furthermore, the commonly used SIR algorithm is tuned using ad hoc methods in order to reduce the effects of noise and the filtering artifacts imposed by the aperture functions. These ad hoc methods make it difficult to analytically evaluate the quality of the estimates. An estimator that uses the noise distribution can be expected to perform better, is theoretically more appropriate, and allows the quality of the estimates to be analyzed using standard estimation theory tools. Furthermore, this approach can be extended to handle nonlinearities, such as those involved in scatterometer ocean vector wind field estimation.

This paper treats scatterometer image reconstruction as the inversion of a noisy aperture-filtered sampling operation. The sampling model is presented and the appropriate reconstruction sample spacing is explained. A reconstruction estimator based on maximum a posteriori probability (MAP) estimation is proposed for σ^0 imaging from scatterometers. Examples from the Advanced Wind Scatterometer (ASCAT) and the SeaWinds scatterometer are illustrated.

2. SAMPLING MODEL

Scatterometers sample a two-dimensional continuous σ^0 field $s(x)$ with distributed aperture functions $A_n(x)$, which may have a different functional form (shape) for each sample. This produces the sampling operation

$$\vec{g} = \begin{bmatrix} \int A_1(x)s(x)dx \\ \vdots \\ \int A_N(x)s(x)dx \end{bmatrix} \approx \begin{bmatrix} \vec{A}_1^T \vec{s} \\ \vdots \\ \vec{A}_N^T \vec{s} \end{bmatrix} = \mathbf{A} \vec{s}$$

where \vec{g} represents the aperture-filtered samples (i.e., the vector of noise-free σ^0 measurements), \mathbf{A} is a matrix operator that operates on the conventional, regularly spaced samples \vec{s} of the bandlimited version of the continuous-index signal $s(x)$, the \vec{A}_n 's represent conventional sampling of the bandlimited versions of the aperture functions, and T represents the transpose. It can be shown that if the aperture functions

are all bandlimited, the approximate equality becomes an exact equality. The same result is obtained if $s(x)$ is bandlimited even if each $A_n(x)$ is not bandlimited where the rows of \mathbf{A} are conventional samples of bandlimited versions of the aperture functions. Moreover, if $s(x)$ or each $A_n(x)$ is bandlimited and periodic then \mathbf{A} is a finite-dimensional matrix and can be analyzed with standard linear algebra.

The optimum regular sample spacing and optimum bandlimit to use when reconstructing the σ^0 image have not been extensively explored in the literature. Nevertheless, a bound on the frequency recoverability is given in [2]. The bound is determined by the sampling density, suggesting that the reconstruction grid resolution be a function of the density of the aperture-filtered samples. In order to avoid aliasing, the sample spacing must be determined by the bandlimit, or approximate bandlimit, of the aperture functions rather than by the density of the aperture-filtered samples. The density of the samples is related to the condition of the sampling matrix \mathbf{A} (whether it is overdetermined, fully determined, or underdetermined) and does not directly impose a bandlimit on the signal.

3. SCATTEROMETER MAP RECONSTRUCTION ESTIMATOR

Scatterometers are designed for large scale ocean wind vector measurements rather than σ^0 imaging. As a result, scatterometer sampling operators may be underdetermined in imaging applications. Therefore, some signal structure must be imposed in order to estimate the uniform samples of the σ^0 image. This can be done with model-based estimation using a signal model, variational analysis applying additional cost functions, or Bayes estimation employing a signal prior. Here, we take a Bayesian approach and apply a prior using a maximum a posteriori probability (MAP) estimator.

Reconstruction is accomplished by estimating the conventional (uniformly spaced) samples \vec{s} of the σ^0 field using a MAP estimator. The MAP estimator searches for the conventional samples \vec{s} that maximize the maximum-likelihood function scaled by the prior. This process is equivalent to maximizing the linear combination of the log-likelihood function and the log of the prior. The maximum-likelihood function is the probability density function (pdf) of the noisy σ^0 measurements and the prior is a pdf of the σ^0 image.

Noisy scatterometer σ^0 measurements can be represented as Gaussian random variables where the variances are quadratic functions of the means [3]. This noise distribution embodies the receiver noise as well as fading. Measurements are assumed to be statistically independent. The covariance \mathbf{R} of the vector of σ^0 measurements is a diagonal matrix and each diagonal element $R_{i,i}$ can be expressed as

$$\begin{aligned} R_{i,i} &= \alpha_i(\vec{g}_i)^2 + \beta_i\vec{g}_i + \gamma_i \\ &= \alpha_i(\vec{A}_i^T \vec{s})^2 + \beta_i\vec{A}_i^T \vec{s} + \gamma_i \end{aligned}$$

where $g_i = \vec{A}_i^T \vec{s}$ is the i^{th} noise-free σ^0 measurement, and α , β , and γ are parameters that are a function of the scatterometer design and the measured receiver noise power [3]. This noise model results in the MAP log-likelihood objective function

$$L_{MAP} = -\sum_i \left[\frac{(g_{v,i} - \vec{A}_i^T \vec{s})^2}{2R_{i,i}} + 1/2 \log\{2\pi R_{i,i}\} \right] + \log P(\vec{s}) \quad (1)$$

where $P(\vec{s})$ is the prior pdf. We use a log-normal prior with a mean as the AVE image and a tunable variance. A tunable variance allows a trade-off between resolution enhancement and noise amplification.

The local maxima of the MAP objective function can be found by setting the gradient equal to zero and solving the corresponding system of equations. However, the resulting system of equations is somewhat complicated so we use a gradient search method to find a local maximum of Eq. 1 near an initial guess. The gradient search method begins with an initial value computed using the AVE algorithm and moves incrementally in the direction of the gradient until convergence to the maxima.

4. SEAWINDS AND ASCAT EXAMPLES

In this section, two-dimensional reconstruction of the σ^0 field from the SeaWinds scatterometer and the Advanced Wind Scatterometer (ASCAT) is explored. Basic information about SeaWinds and ASCAT is presented, the optimal regular sample gridding is derived from the aperture functions, and an example is provided.

SeaWinds is a Ku-band scatterometer that orbits the Earth in a sun-synchronous near-polar orbit. The instrument has a scanning pencil-beam antenna with two beams at different incidence angles and polarizations. The v-pol beam is at a nominal incidence angle of 54 degrees with the h-pol beam at an incidence angle of 46 degrees. This produces a swath with four 'flavors' (v-pol fore- and aft-looking and h-pol fore- and aft-looking) in the inner portion of the swath and two flavors in the outer portion of the swath where there is only one beam. The backscatter return from each pulse from each beam is partitioned into several 'slices' using range-Doppler processing. Each slice is considered to be statistically independent and each has its own aperture function or slice spatial response function [4].

The ASCAT scatterometer is a C-band v-pol instrument in near polar orbit that has two sets of three stationary fan-beam antennas pointed at different azimuth angles. The system applies a type of pulse compression to obtain range resolution, producing slice σ^0 measurements with a relatively wide range of incidence angles. This sampling results in a swath in which each point is sampled by multiple beams with differing azimuth angles [5].

The σ^0 measurements represent noisy aperture-filtered samples of the two-dimensional σ^0 field. The σ^0 field may be reconstructed using the various slice measurements of a similar flavor (i.e., having the same geometry, frequency, and polarization). Measurements of a given flavor sample the same σ^0 field and can be combined. Furthermore, for land and ice imaging purposes, all slices of a given polarization and frequency may be combined by assuming negligible azimuthal variation and by adjusting the σ^0 values to a common incidence angle [1]. Depending on the application, multiple passes may be combined to increase the sample density and reduce noise. For SeaWinds, the incidence angle adjustment is not necessary since the slices of a given polarization have a similar incidence angle. For ASCAT, incidence angle normalization to 40° is used.

The image grid pixel size is determined by the bandlimit of the slice spatial response functions. Figure 1 illustrates typical 6dB contours of the slice spatial response functions for a given pulse from SeaWinds and from ASCAT [6] [7]. For SeaWinds, the 6dB slice contours are approximately 6km in the narrow direction and 25km in the long direction. For ASCAT, the contours are about 4.2km in the narrow direction and 20-35km in the long direction. In the following, each of the slice response functions is approximated by a sinc-squared function that has the same 6dB width as the slices in the narrow and long directions. The sinc-squared functions can be represented by regular samples with spacing corresponding to about half the narrow 6dB beam-width. This sample spacing is scaled by a factor of $1/\sqrt{2}$ to allow for the worst-case slice orientation with respect to the gridding axes (i.e., 45°). For SeaWinds, this results in a conventional sample spacing of about $6\text{km}/2\sqrt{2} \approx 2.12\text{km}$ [8]. For ASCAT, the conventional sample spacing is about $4.2\text{km}/2\sqrt{2} \approx 1.5\text{km}$. Note that the range filtering of the σ^0 values done onboard the ASCAT spacecraft degrades the effective reconstruction resolution. Thus for ASCAT, a coarser conventional sample spacing may be appropriate.

Figure 2 shows multi-orbit gridded, SIR, and MAP images of the Amazon made from SeaWinds and ASCAT data. For ASCAT, the incidence-angle-normalized images are plotted. As expected, the ASCAT effective resolution is lower due to the onboard spatial filtering. The results of the reconstruction algorithms, represented by the bottom two rows of images in Fig. 2, enhance the resolution compared to the gridded product (top row). The MAP images (bottom row) contain more detail than the SIR images (middle row), although the MAP images seem to be noisier. The noise in the MAP images can be attenuated by filtering the images or by tuning the variance of the log-normal prior, which can produce images of comparable quality to the SIR images.

Figure 3 shows a false color MAP image of the Weddell Sea in Antarctica using four days worth of data from SeaWinds and ASCAT. The differences in polarization and frequencies between the different data sets allow discrimination

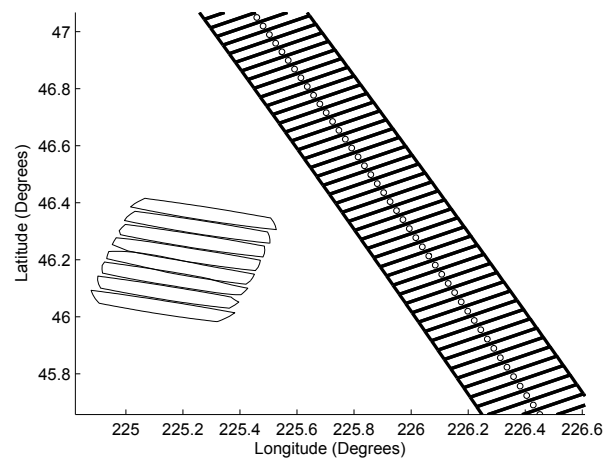


Fig. 1. Typical slice spatial response functions from SeaWinds and ASCAT for one pulse. The 6dB contours are shown. The boxes with the circles in them are ASCAT slices; the contours on the left are SeaWinds slices.

between different types of surfaces. The blue region in the top left corner is open ocean, the purple regions of the image are newly formed sea ice, whereas the tinted yellow regions are older, thicker sea ice. The brighter yellow region in the lower left is the Ronne ice shelf. The bright white regions are glacial ice on the Antarctic peninsula and large icebergs embedded in the sea ice. Combined, the two scattermeters offer more discrimination capability than either alone.

5. CONCLUSION

This paper considers signal reconstruction from aperture-filtered samples, focusing on scatterometer σ^0 imaging. A new reconstruction algorithm is proposed based on MAP estimation, which deals appropriately with noise. Examples from SeaWinds and ASCAT are presented. Posing the problem as the inverse of a discrete aperture-filtered sampling operation allows for a bound on the resolution enhancement. Thus, the optimal pixel resolution corresponds to the highest bandlimit of the aperture functions. The new MAP method enhances the resolution without introducing ad hoc processing steps. The quality of the MAP estimates may be analyzed with standard estimation theory. The MAP reconstruction approach can be extended to handle nonlinearities, allowing for ocean wind vector field reconstruction.

6. REFERENCES

- [1] David G. Long, Perry J. Hardin, and Peter T. Whiting, "Resolution enhancement of spaceborne scatterome-

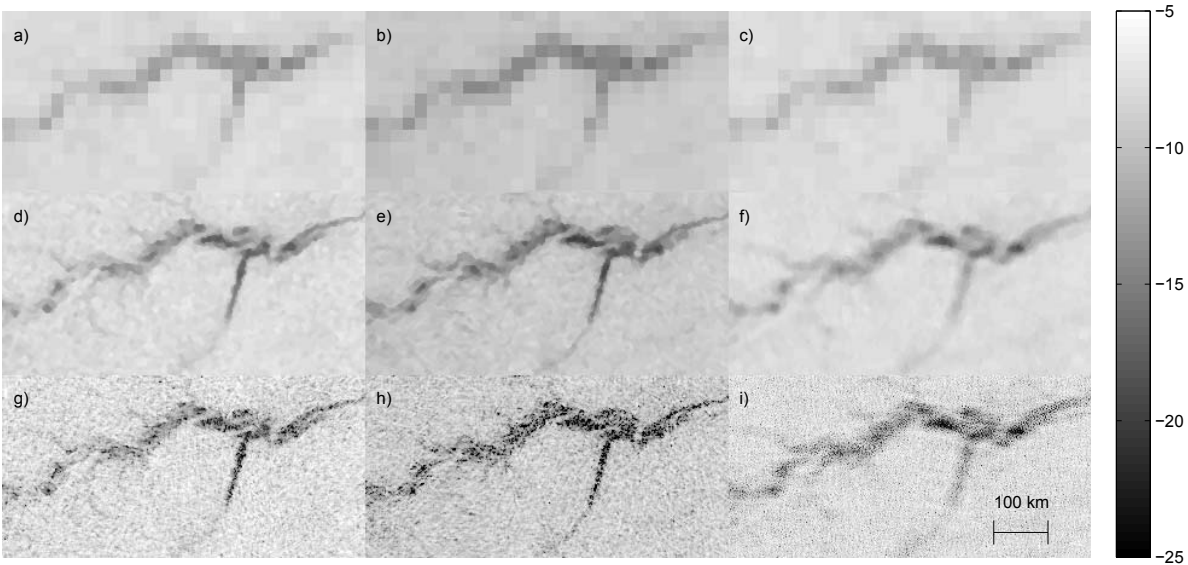


Fig. 2. Reconstructed σ^0 images (in dB) from SeaWinds and ASCAT over the Amazon using four days worth of data (JD 201-204) in 2008. Images a), b), and c) are gridded images of SeaWinds h-pol, SeaWinds v-pol, and ASCAT, respectively. Images d), e), and f) are SIR images of SeaWinds h-pol, SeaWinds v-pol, and ASCAT, respectively. Images g), h), and i) are MAP images of SeaWinds h-pol, SeaWinds v-pol, and ASCAT, respectively. The diagonal streaks in the river are actual features.

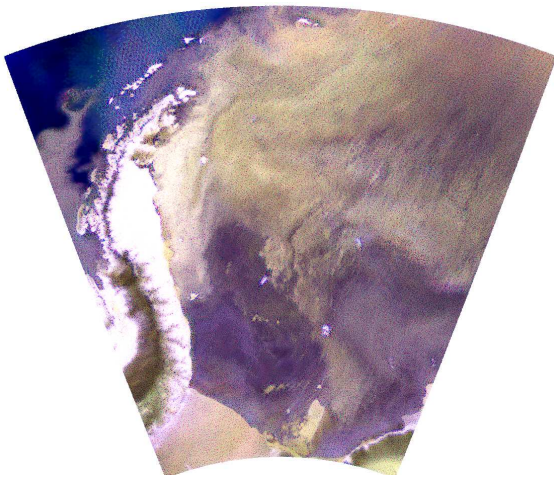


Fig. 3. False color MAP reconstructed σ^0 image from SeaWinds and ASCAT over the Weddell Sea in Antarctica using four days worth of data (JD 201-214) in 2008. Red corresponds to the SeaWinds h-pol image, green corresponds to the SeaWinds v-pol image, and blue corresponds to the ASCAT image.

ter data,” *IEEE Transactions on Geoscience and Remote Sensing*, vol. 31, 1993.

- [2] David S. Early and David G. Long, “Image reconstruction and enhanced resolution imaging from irregular samples,” *IEEE Transactions on Geoscience and Remote Sensing*, vol. 39, no. 2, pp. 291–302, 2001.
- [3] Robert E. Fischer, “Standard deviation of scatterometer measurements from space,” *IEEE Transactions on Geoscience and Remote Sensing*, vol. GE-10, no. 2, April 1972.
- [4] Ted Lungu, *QuikSCAT Science Data Product Users Manual Overview and Geophysical Data Products*, September 2006.
- [5] *ASCAT Wind Product User Manual*, August 2009.
- [6] Ivan S. Ashcraft and David G. Long, “The spatial response function of SeaWinds backscatter measurements,” in *Proceedings of SPIE*, William L. Barnes, Ed., SPIE, Bellingham, WA, Aug 2003, vol. 5151.
- [7] Richard Lindsley and David G. Long, “Adapting the SIR algorithm to ASCAT,” *IGARSS*, 2010.
- [8] Brent A. Williams, Michael P. Owen, and David G. Long, “The ultra high resolution QuikSCAT product,” in *Proceedings of the 2009 IEEE Radar Conference*, Pasadena, CA, May 2009, IEEE.